9-1-2011

The Evaluation of a Biologically Inspired Engineered MAV Wing compared to the Manduca Sexta Wing under Simulated Flapping Conditions

Nathanial DeLeon

Anthony N. Palazotto
Air Force Institute of Technology

The Evaluation of a Biologically Inspired Engineered MAV Wing Compared to the *Manduca Sexta* Wing under Simulated Flapping Conditions

Nathanial E. DeLeón, 2d Lt USAF **Dr. Anthony Palazotto, Professor**
Air Force Institute of Technology

Received on 24 June 2011; Accepted on 24 August 2011

ABSTRACT

In recent years, researchers have expressed a vested interest in the concepts surrounding flapping wing micro air vehicles (FWMAVs) that are capable of both range and complex maneuvering. Most research in this arena has found itself concentrated on topics such as flapping dynamics and the associated fluid-structure interactions inherent in the motion; however there still remain a myriad of questions concerning the structural qualities intrinsic to the wings themselves. Using nature as the template for design, FWMAV wings were constructed using carbon fiber and Kapton and tested under simplified flapping conditions by analyzing `frozen' digital images of the deformed wing by methods of photogrammetry. This flapping motion was achieved via the design and construction of a flapper that emulates several of the kinematic features that can be seen in naturally occurring flyers. The response to this motion was then compared to the inspiring specimen's wings, the North American Hawkmoth (*Manduca Sexta*), under the same flapping conditions in order to identify some of the key features that nature has deemed necessary for successful flight. Results showed that though the engineered wing emulated several of the structural characteristics of the biological wing; it still required some design modifications to compare more closely to the biological wing in the flapping motion. Additionally, this research also speaks to the effects of air on the biological wing.

1. INTRODUCTION

1.1. Motivation

In terms of tactical advantage on the battlefield, the realm of micro air vehicles (MAVs) shows promise. As warfighters are taxed with ever increasingly difficult situations, it is crucial that they be made aware of what is to come; whether it be over a hill, in a cave, or in a room of an unknown building [1]. The MAV will be capable of a multitude of close quarter reconnaissance tasks, ranging from battlefield operations to safety inspections of civilian structures [2]. The Defense Advanced Research Project Agency (DARPA) solidifies and enumerates some of the specifics associated with the projected MAV as is shown in Table 1 [2].

The vision of the optimal, operational MAV as outlined by DARPA allows for creativity in the construction of this machine despite the specific constraints. The realization of practical MAV applications is possible due to the ever-decreasing size and weight of payload components such as video cameras, chemical sensors, and autopilots [3]. One issue that does present itself is the subject of maneuverability. The MAV, as required by DARPA, should have the ability to negotiate small spaces and perhaps even hover within close quarters; a near impossible feat for a vehicle that requires forward motion. When indoors, slower is better [4]. This realization leads one to a nonconventional concept that has yet to be achieved by man: flapping flight. It can be said that it is perhaps necessary to turn to nature for answers as it has already found the ability to create small, agile flying machines. Particular interest is found within insects due to the fact that the wings themselves are rigid and are passively controlled. Those in Norris *et al* [5] stated that prior to the mid 1990's there existed serious interest in the realm of

flapping, however only about 10% of the research conducted dealt with wing structures. Current research finds a vested interest in this *flapping wing* MAV (FWMAV), however science is compelled to mimic the elegant (and perhaps efficient) designs that nature has already employed for its flapping wing design [5]. Nothing in nature exhibits fixed wing flight behavior or propeller driven thrust, rather it is flight through flapping that perhaps is the key to the successful creation of the MAV [4].

Table 1. MAV Specifics as Outlined by DARPA [2]

Specification	Requirements	Details
Size	<15.24 cm	Max Dimension
Weight	~100 g	Objective GTOW
Range	1-10 km	Operational Range
Endurance	60 min	Loiter Time on Station
Altitude	<150 m	Operational Ceiling
Speed	15 m/s	Max Flight Speed
Payload	20 g	Mission Dependent
Cost	$1,500	Max Cost, 2009 USD

GTOW- Gross Takeoff Weight, USD- United States Dollar

1.2. Biological Inspiration

This research aims to further investigate the structural aspects of the FWMAV wing, specifically one in which is biologically inspired. The medium of inspiration is achieved by the North American Hawkmoth (*Manduca Sexta*) due to its availability and size [1] [5]. Additionally, the *Manduca Sexta* exhibits remarkably consistent wing beat characteristics [6] during flight, making it the ideal candidate for consideration as this fact eliminates some of the variability that can be considered influential to flight through flapping [5]. Figure 1 shows a picture of the inspiring specimen and the wing associated with it.

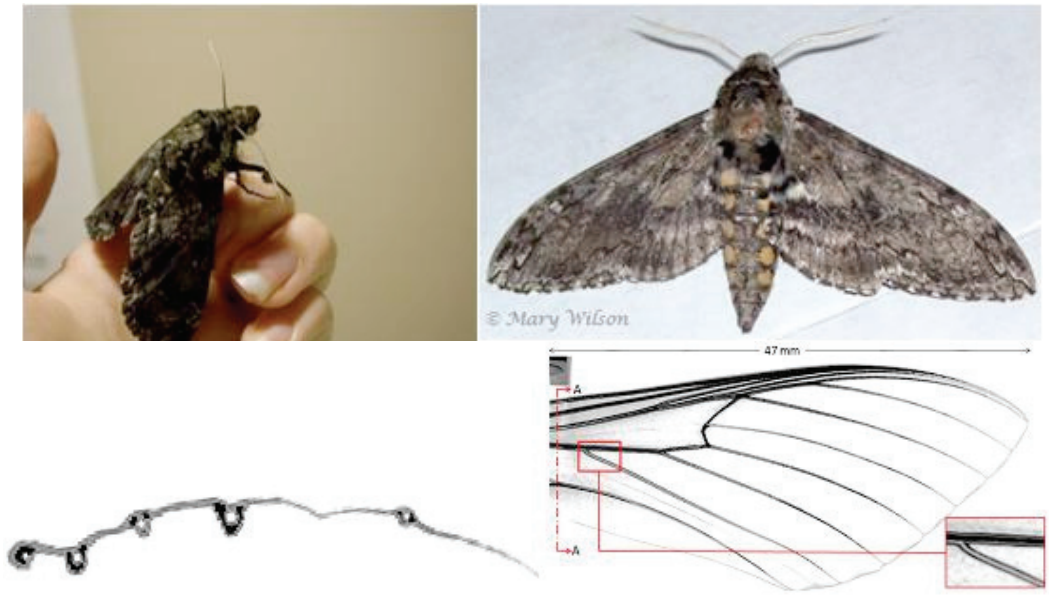

Figure 1: North American Hawkmoth (Top) and Computed Tomography Scan Image of Forewing Cross-Section (Lower Left) and Top (Lower Right)

Figure 1 serves to show some of the geometric characteristics of both the moth[1] and the forewing. The main function of any biological being or any flying object for that matter is to transmit energy to the

[1] All moth specimen tested were provided courtesy of Dr. Mark Willis of Case Western Reserve University

external environment during flight in order to become airborne without risking damage to the flight vehicle itself in the form of bone or muscle damage [7]. This requires that both structure and the materials used to construct it must be specific to their purposes. It should be of no surprise that nature integrates varied methods of construction when it comes to the fabrication of materials used as support structures. Figure 1 shows both the top view of a *Manduca Sexta* wing, along with a crossectional view of the wing at the half chord[2] . The general shape of the wing is similar to that of other biological beings in the Insecta class, such as the dragonfly and cicada, both of which can be considered model fliers for MAV application [8]. The materials used in the biological speciemen are currently under investigation [9], however it can be said that the wing is composed of two main materials, albeit there are the presence of a 'membrane' that acts as a matrix between 'vein' elements. The veins primarily are made out of a material known as *cuticle* which is a fibrous composite material. The fibrous component consists of micro fibrils of *chitin*, a polysaccharide, and the matrix is protein. Wooton [10] mentions that the chitin is generally chemically uniform throughout the insect world, but the matrix of protein varies greatly, disallowing the assumption of universal insecta material properties.

Those in Norris *et al* [5] recognized the value in using the *Manduca Sexta* as the model flapping flier and executed a rigorous investigation of the structural aspects of the biological wing via the modal analysis. Inspired by the works of Combes and Daniel [11] [12] [13] and others, they too felt that the structural aspects of the flapping wings required further study. They were particularly interested in the consistencies that were seen from specimen to specimen. Using a scanning laser vibrometer (SLV), Norris *et al* [5] obtained the resonant frequencies (results shown later) of separated Hawkmoth wings in both air and vacuum in order to gage the *dynamic stiffness* of the wings. His near consistent results led him to believe that the slight scatter of results allowed for a larger tolerance of parameters in construction wherein 'close is good enough' for parameter modeling. This grants some leeway in the fabrication process and speaks to the possibility of damage sustainability [5] of the wings.

In addition to their findings, Norris *et al* [5], Combes and Daniel [11] [12] [13], and Ennos [14] [15] all expressed interest in the aeroelastic response of the wing, specifically questioning the dominance of inertial (mass distribution dominated) or aerodynamic (pressure distribution dominated) effects on the wing behavior. This was coined by Norris *et al* as *The Aeroelastic Question*. Though those in Norris *et al* primary concentration lay deeply in the modal analysis of the wings, they did employ methods of photogrammetry in a similar fashion to that of Combes and Daniel (see [13]) and Willmont and Ellington (see [16]) wherein two dimensional images were taken of flapping wings at several angles to reconstruct their three dimensional coordinates/orientations. This methodology clearly provides the basis of thinking for this study.

1.3. Basis of Investigation

Using the combination of several experiments as the basis of methodolology (Norris et al [5], Combes and Daniel [13] and Willmont and Ellington [16]), this study aims to investigate the aspects of the wing that are most important in the construction of a FWMAV. Here, a biologically inspired flapping wing was constructed. The parameters of the biological wing that were chosen to be emulated by the engineered wing were the size, vein geometry, mass, and the first resonant frequency (refered to as the first bending mode by those in Norris *et al* [5]) . This wing, along with a separated biological wing, was subjected to both a modal analysis and a dynamic flapping analysis. The flapping motion was achieved by constructing a flapping mechanism based on biological inspiration and was placed in a vacuum chamber for both an air and vacuum test. The response of the two wings to the flapping motion was captured by photographing 'frozen' images (via stoboscopy) at several angles of observation to obtain the three dimensional characteristics of the deformed/deflected wings.

2. MANUFACTURING

The manufacturing process of the biologically inspired engineered wing was an iterative process that was taken through several design considerations (for more information on several of the design iterations, see DeLeón *et al* [8]). The finalized design incorporated the adhesion of three layer, cured carbon fiber that was layed up in a 0-90-0 configuration for a total thickness of .16 mm and 20 µm Kapton film. The vein formation was extracted by cutting the geometry into the carbon with a laser. A standardized process of wing removal from the *Manduca Sexta* also had to be considered due to the fact that comparisons had to be made.

[2] Images gained from computed tomography (CT) scan courtesy of the Air Force Materials Directorate

2.1. Biological Wing Removal

In order to more accurately compare the response of the inspiring specimen to that of its engineered counterpart, it was necessary to standardize the methods associated with the removal of the wing. It is important to realize that there is a distinct time dependency associated with a removed wing. Both those in Norris *et al* [5]and Combes and Daniel [11] [12] make mention of this issue in that the wing will essentially 'dry out' upon removal from the living creature. Both sources indicate that a wing can be deemed 'useless' within three hours of being removed in that its structural properties appear to stiffen and become more brittle, much like a tree branch that has been removed. Recent observations indicate that the wing actually begins to form an unnatural camber within 30 minutes of removal, which can be compared to that of a drying flower petal that curls when exposed to sunlight. It can thus be stated that the methods of removal must be executed quickly in order to preserve the integrity of the wings properties. The experiments here were executed within 1hr, 42 mins.

Wing removal began by cutting into the *thorax* and removing the wing *and* the shoulder, preserving as much of the structure as possible. Following removal, the wing scales were removed in order to remove mass and account for the addition of the reference points that will be discussed later. Figure 2 shows the cut location and the removed wing.

Figure 2: Cut Location and Removed/de-scaled Manduca Sexta Forewing

Following the removal of the wing, reference points were added to the wing surface in standardized locations on both sides. Further details on this process will be discussed in section 2.3.

2.2. Carbon Fiber Configuration and Obtaining the Vein Structure

The two dimensional vein orientation was achieved by observing a two dimensional image of the CT scanned biological wing. Points were identified along the vein geometry and then splined through using a 2-D spline in a MATLAB code designed by Ryan O'Hara (see [9]) to construct the vein orientation. Here, the vertices were selected using MATLAB's built in image recognition software. These vertices could then be loaded into a computed aided design program SolidWorks, Corel Draw, and MATLAB now incorporates at ™ in order to generate a three dimensional model of the vein formation. The layout could then be applied to Corel Draw, which would allow for the Epilog 45 Watt CO_2 laser to cut out the formation. Figure 2 depicts the formation of the cutout and the laser used to perform the cuts.

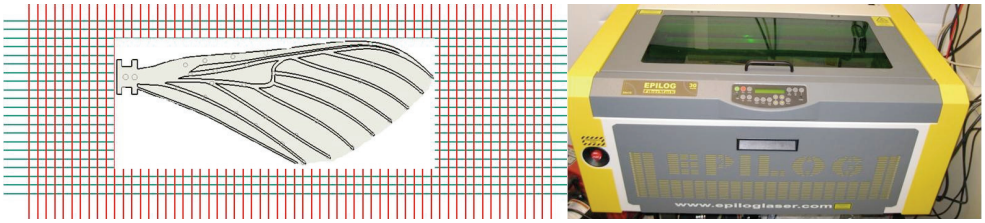

Figure 3: Carbon Fiber Layup and Cut Demonstration and Epilog Laser

It should be stated that unlike the methods discussed by Xie and others [17] wherein the carbon fibers were aligned with the vein geometries, the veins were simply constructed from this cutout. This will

yield non-homogeneous properties along the length of the veins not aligned with the leading edge or the carbon fibers. This adds an aura of complexity to the structural analysis and any finite element simulations of this engineered wing.

2.2. Construction Process

A standardized construction process was conceived for this study in order to make evaluations measurable and repeatable. The carbon fiber laser cutouts of the wing vein geometries were lightly cleaned to remove any residue that had been left by the cutout process. Following this was the application of the adhesive, which was 3M 45 Spray Adhesive applied via a small paintbrush. This allowed for a uniformity in distribution of the adhesive and eliminated the need to apply the adhesive to the whole of the membrane (20 µm Kapton Film), which was stretched over the carbon cutouts and allowed to dry. The extra membrane was removed from around the wing with a scalpel. Additionally, a construction vein that allowed for the trailing edge to end in a membrane like the inspiring specimen was removed. The wing in its entirety was then placed under a stencil that was constructed from thick Kapton film that had standardized manufactured holes in it that would allow for standardized reference point application to the wing (reference points used in photogrammetry and will be discussed later). Figure 4 shows this process in its entirety.

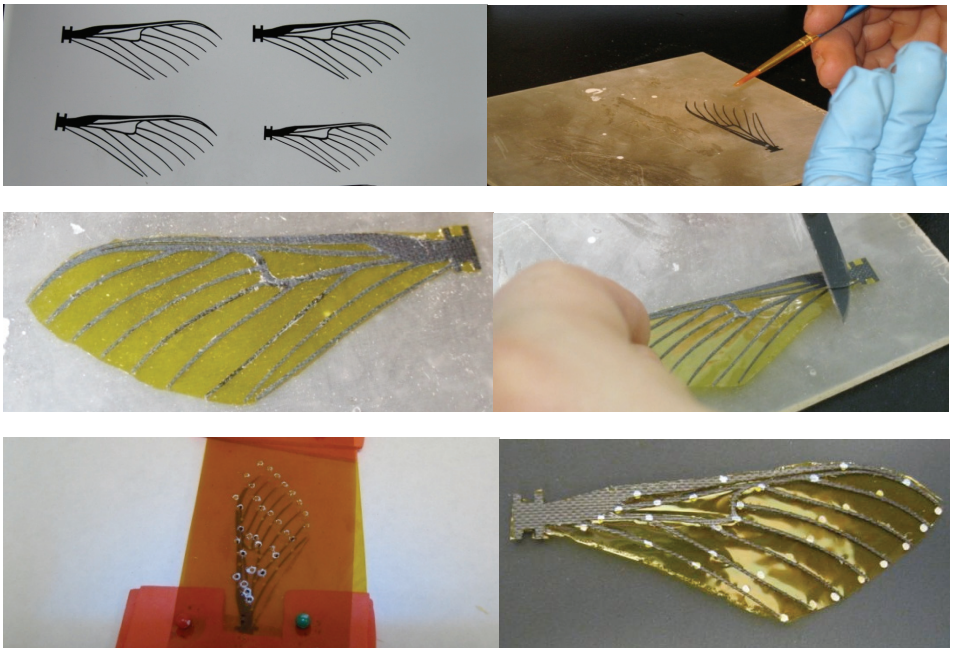

Figure 4: Process of Engineered Wing Fabrication

Concerning the application of reference points, the goal was for them to be non-intrusive in terms of mass and first bending mode. Combes and Daniel claim that if reference points were to be applied, they must affect the total mass by no more than 2% [13], which would affect the first bending mode by no more than 1%. Several avenues were considered for the material used for reference points, to include those found in Willmont and Ellington's experiments [16], fluorescent dyes, and *Sharpie*^{TM} markers. The material that proved to be the most condicive in terms of mass and modal analysis was the *Pentel*^{TM}*WHITE 100WS Fine Marking Pen*, which could mark on both wings.

2.3. System Identification and Comparision of Wings from a Modal Standpoint

The crux of this study was to re-examine the realm of the structural characterization of the *Manduca Sexta* wing and compare it to that of one that was designed and constructed by man with nature in mind. Previous research ([5] , [1], [2]) held the modal analysis as the end all-be all of structural characterization. Initial conjectures that revolved around this study viewed these claims with skepticism since the small displacements inherent in the modal analysis do not find themselves as a part of the functionality of these wings.

Despite doubt, it was deemed pertinent to characterize the biological wing under these several conditions via the modal analysis. This action secures its necessity due to the fact that before this study, there was no solid method of structural characterization beyond what was seen in Combes and Daniel [11] and [12] and Norris *et al* [5] as stated earlier. Using a scanning laser vibrometer, this modal analysis was carried out to yield the values shown in Table 2.

Table 2

Wing	Mass (Clean)	Mass (WRP)	1st Mode (air)	2nd Mode (air)
Biological	73.3 mg	68.5 mg	64.75 Hz	110.75 Hz
Engineered	61.7 mg	62.0 mg	59.06 Hz	78.13 Hz

WRP- With Reference Points

In order to more fully understand the results of the modal analysis, Figure 5 shows the first four mode shapes of the biological wing along with the masses of each of the wings.

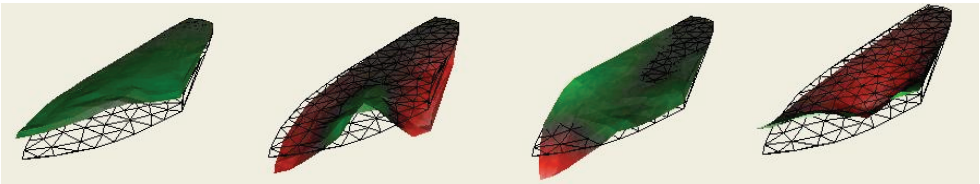

Figure 5: First Four Mode Shapes of Biological Wing in Air

The mode shapes grant a glimpse of the behavior of each of the resonant frequencies. In Figure 5, the black grid represents the original wing surface and the colored grid represents the mode shapes of the wings. The first mode shows bending, and the second is torsional. Table 2 sheds light on the comparability between the two wings. In terms of mass, it would appear that the wings compare well. It should be noted that the shoulder was considered to be a part of the mass however the shoulder member of both wings was clamped as will be shown in Figure 10. It should be pointed out that for the biological wing, mass was lost during the reference point application process (which lasted 7 minutes). This loss of mass was indicative of the aforementioned time dependent behavior of the wing. In terms of the resonant frequency, the engineered wing held a 7.8% difference in the first mode and a 29.6% difference in the second. What can be gleaned from these values are that the wings are similar, however stifness may be lacking in the engineered wing in the chordwise direction.

3. EVALUATION

In order to evaluate the response of the engineered wing and the biological, it was necessary to devise a standardized and repeatable process of experimentation so that the wings could be tested in both air and vacuum. Here, a photogrammetry package known as Photomodeler™ was used in concordance with the reference points applied to the wings to evaluate the wings' responses to flapping motion, which was achieved by the construction of a flapping mechanism designed to mimic the kinematics of a flapping Hawkmoth. The image capturing for photogrammetry was achieved via stroboscopes, which was set to evaluate 12 different angles throughout the stroke amplitude (6 in the downstroke and 6 in the upstroke). Each specimen was subjected to flapping in both air and vacuum in both air and vacuum for three trials as is shown in Table 3.

Table 3

Wing	Angles Per Stroke	Air	Vacuum	Trials	Total Trials
Biological	12 angles	1	1	3	72
Engineered	12 angles	1	1	3	72

3.1. The Flapper

A flapping mechanism was designed based off of the kinematics and design of the *Manduca Sexta*. Figure 6 [18] shows the progression of thought in the design of the mechanism which is meant to mimick what is seen on the inspiring specimen.

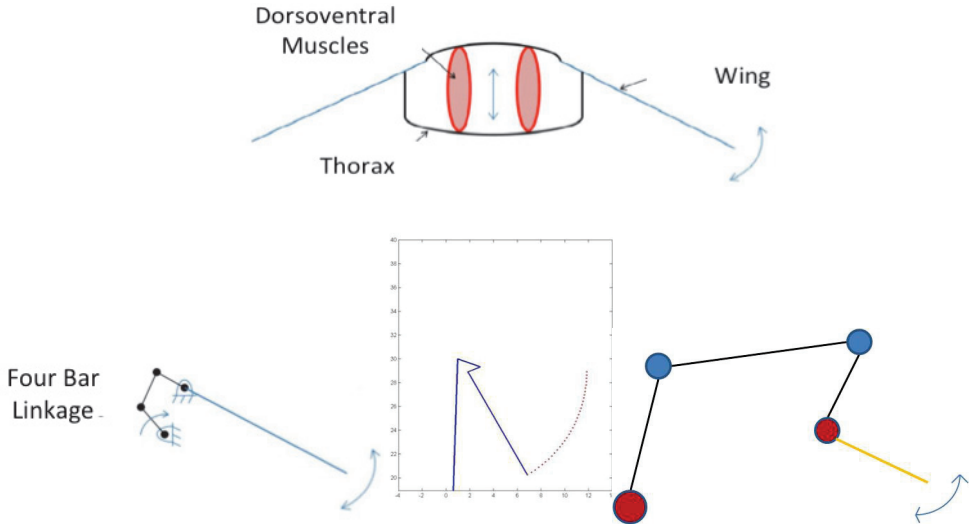

Figure 6: Biological Design as Approximated by Four Bar Mechanisms

The top picture in Figure 6 shows the biological design. The bottom left and middle show how a Crank-Rocker mechanism can be used to approximate the kinematics of the inspiring design as seen by those in Anderson *et al* [18] who used piezoelectric materials to achieve the flapping motion. This study uses this concept by achieving similar motion by using mirrored Crank-Rocker mechanisms. Figure 7 shows the kinamatic breakdown of the flapping mechanism with the associated SolidWorks given a^{TM} conception.

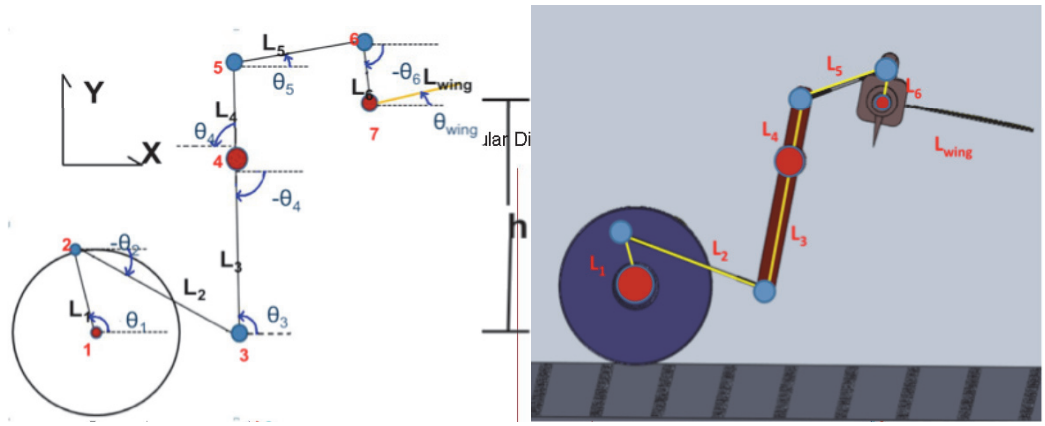

Figure 7: Mirrored Crank-Rocker Mechanism For Flapping Motion

The total flapping amplitude achieved by this design was 107.9 degrees. This was based off of data taken from Willmont and Ellington [16] which measured the flapping amplitude of a flying *Manduca Sexta* and traced a point off of the leading edge of the wing. Figure 8 shows a comparison of the rigid body analysis of the flapping mechanism shown here, the flapper previously used made by those in Norris *et al* [5], and the data achieved by Willmont and Ellington. The left plot shows the Willmont and Ellington data as compared to the rigid body analyses of the old and new flapping mechanisms. The right plot depicts the accelerations of the aforementioned data.

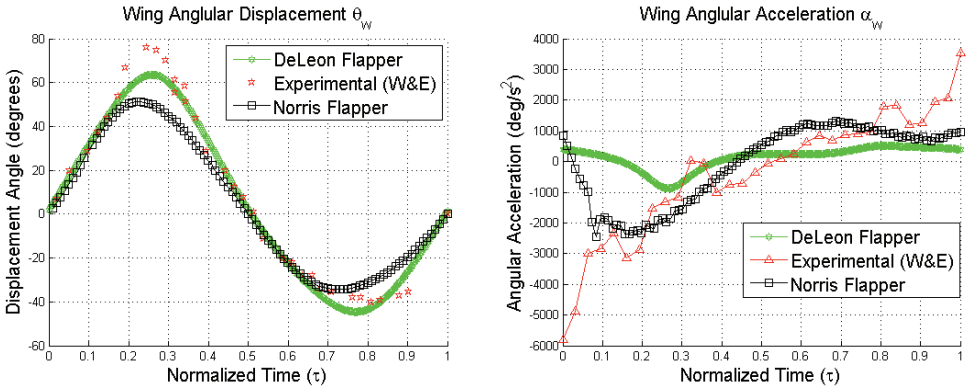

Figure 8: Kinematic Analyses of Flappers Compared to Experimental Data

A regression analysis was carried out to reveal that in terms of angular displacements, the flapper shown in Figure 7 compares better than the flapper conceived by Norris *et al* [5]. In terms of angular accelerations however, the flapper shown in 7 exhibits far lower amplitudes than that of the biological or flapper conceived by Norris *et al* in [5]. One possible advantage of this lack of amplitude would be the fact that less force would be applied to each wing tested in the new flapper, thus allowing for more wings to be tested.

The final flapping mechanism is shown in Figure 9. The flapper was materialized using the Connex 500 3d Printing machine, which places 16 µm layers of a photopolymer down at a time to construct a 3d object based off of a 3d CAD drawing. In order to drive the mechanism, and MPI HIMAXX 600 Watt brushless motor was used in conjunction with a *Pheonix*^{TM} ICE 50 speed controler.

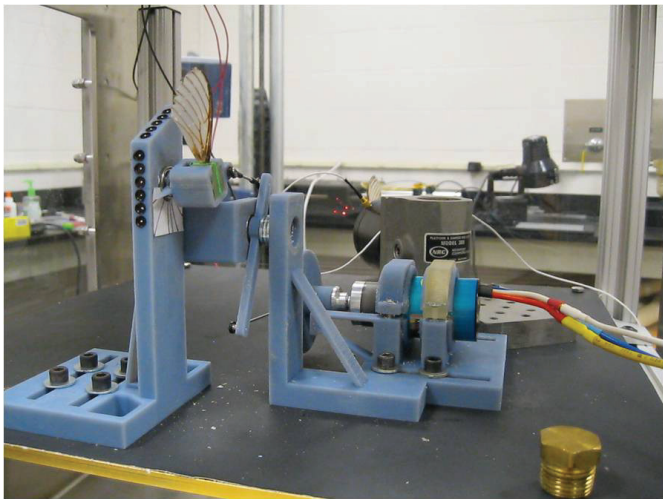

Figure 9: Physical Flapping Mechanism

Atop of the flapping mechanism are additional, non-translating reference points that were manufactured into the flapping mechanism for the purpose of scaling and axis determination in the photogrammetry process.

Another detail of the flapping mechanism tht should be stated would be the boundary condition that acted as the interface between wing and flapper. The clamp used was considered a rigid clamp [1] in that the wing would sit in between two manufactured pieces that were lined with a foam that would allow for some give in the flapping motion. This configuration, which was also used by those in Norris *et al* [5], can be seen in Figure 10.

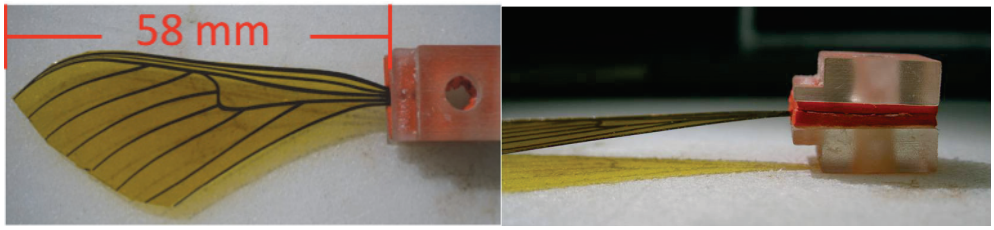

Figure 10: Depiction of the Rigid Clamp Incorporated for Analysis

Though the clamp in Figure 10 does not accurately mimic the boundary condition of the insect, it did provide a simplified, standardized method of evaluation that could be applied to both wings regardless of geometry.

3.2. Experimental Setup

The basic premise of this study is a comparison of the manufactured wing to the biological wing. However, there is a chance here to also consider the aeroelastic question, a topic that has presented itself throughout this literature and within many more. In order to examine this, it is not only pertinent to flap these wings in air, but also in vacuum. This will serve to evaluate the inherent differences between purely inertial deformations and displacements and those that present themselves only in the presence of aerodynamic effects. Figure 11 shows the experimental setup as a whole.

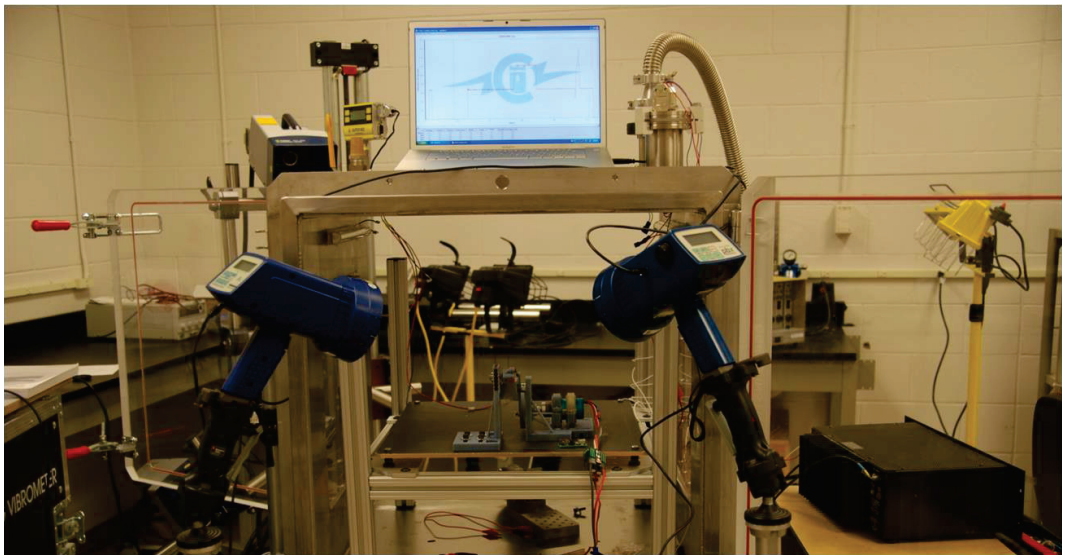

Figure 11: Experimental Setup

The first piece of equipment to consider is one that grants the ability to evaluate in both air and vacuum, be it the vacuum chamber, which is a the center of Figure 11 and will contain both the signal generator (for modal analysis) and the flapper. The same Abbess Instruments Vacuum Chamber was used by Norris *et al* [5], however due to the new flapper, slight modifications had to be made to accommodate the motor. As it turned out, the Phoenix ICE 50 speed controller held within it electrolytic capacitors which cannot handle vacuum conditions. As a result, it was determined that all speed control had to happen *outside* of the the chamber, and thus the speed controller had to be removed. This was done by utilizing one of the vacuum chamber's built in ports that allowed wires to pass through from ambient to the chamber conditions.

On either side of the chamber in Figure 11, two blue light guns can be observed on stands facing flapper inside the vacuum chamber. These are the stroboscopes that have been referred to previously in this paper. Their primary function is to display a 'frozen' image for the purpose of photographing a test subject while flapping. The stroboscopes (two of them were used) used for this experiment were Monarch™ Phaser Strobes. The stroboscopes retained the ability to measure/mimic the phases of moving objects. This was

done via an Optical LED sensor that obtained feedback from a strip of reflective tape on the Flywheel depicted as the driving link in Figure 7. Every time this tape passed the field of the sensor's LED (light-emitting diode) light, the signal generated by the reflection fed phase information to the stroboscope.

3.3. Experimental Procedure

As mentioned, twelve angles/phases throughout the stroke amplitude were observed for this study. The stroboscopes discussed in the previous section, in addition to having the ability to retain phase information, also had the ability to incorporate a *phase delay* from 0-360 degrees. This feature allowed for the observance/gathering of data at the 12 angles, which can be seen in Figure 12 which depicts the rigid body motion of the flapping mechanism, overlayed with vertical lines which represent the angles observed.

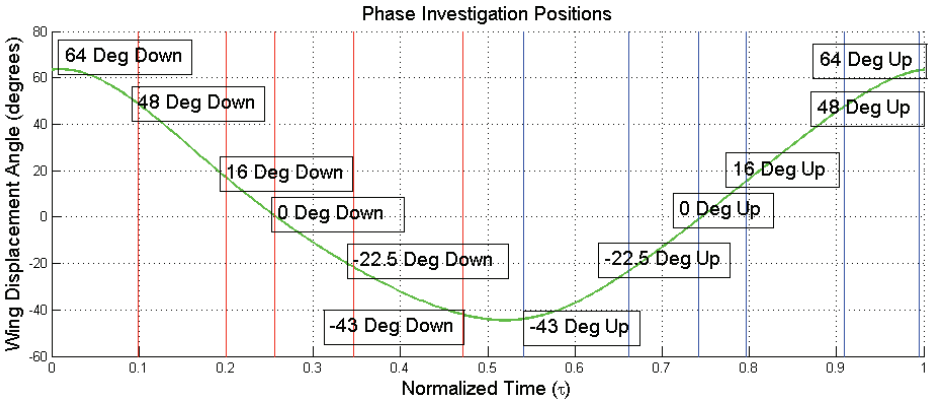

Figure 12: Phases Observed

The wings were first flapped in vacuum, then in air at a flapping frequency of 12.5 Hz. Three pictures were taken of each strobed wing three times (for averaging) for each of the phases shown in Figure 12. The three pictures taken at differet angles of the same phase were used to generate the three dimensional characteristics of the wing's reference point. Photomodeler yielded the coordinates of points in space which could later be used to analyze the wing behavior. Figure 13 grants a glimpse of some of the picture taking methods incorporated in this study, along with examples of some of the pictures that were used for the three dimensional characterization.

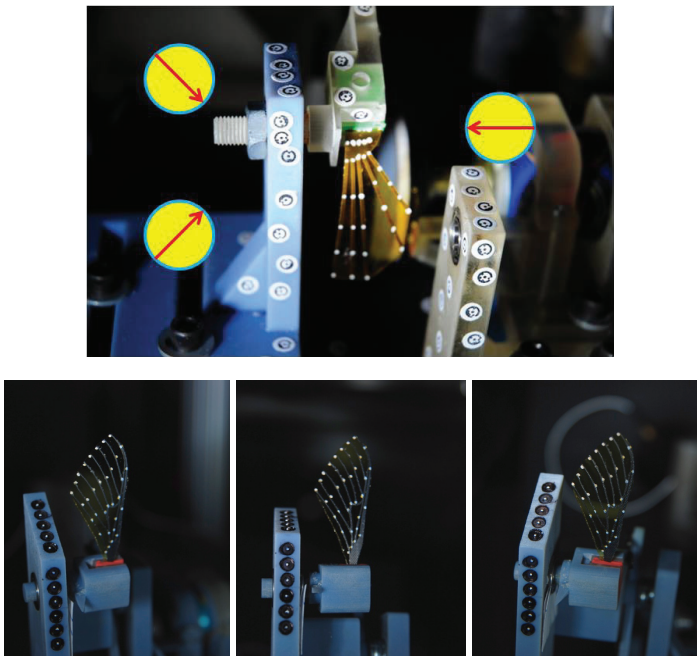

Figure 13: Photomodeler Application Methods

It was conceived that the camera angles depicted in Figure 13 would grant the best resolution in all three dimensions of the 'flapping but frozen wing'. The camera used in the data gathering process was a NIKON D80 with a Promaster^{TM} Digital XR EDO Aspherical LD (IF) 17-50 mm 1:2.8 Macro _ 67 lense. For this operation, the zoom, focus, aperature, and fstop all had to remain fixed for each photograph taken.

Once all the photographs were taken (data gathering) it was then necessary to extract the three dimensional positions of the reference points on the wings. To do this, Phtomodeler^{TM} was utilized in a standardized manner. 44 reference points existed within the system (33 on the wing, 11 nontranslating reference points on the flapper), all of which were identified in each of the photographs, referenced to each other, and then processed for triangulation [19]. The 11 reference points on the flapping mechanism were used to form the axes. Figure 21(at the end of this paper) shows the surface fitted hard photomodeler data of the downstroke and upstroke of both wings flapping at the 48 degree angle.

4. NUMERICAL METHODS

To display the results of the aforementioned procedure, it is necessary to discuss the numerical methods associated with the data extraction. Originally, the goal of the procedure was to execute a 'point-to-point' comparison wherein the three dimensional positions of the corresponding points on the two wings under the two conditions (air and vacuum), would be compared to each other. However the differences in behavior were so vast, that new considerations had to be made. Data was first organized into a manageable fashion, splined through using a Cardinal (Catmul-Rom) Spline [20], then the residuals were analyzed for each point to determine the reliability of the points used. Then the torsional and angular displacements were considered via a vector analysis.

4.1. Cardinal Spline

A cardinal spline interpolant is not a new method of splining, rather it utilizes the averaging methods incorporated in such processes as `overlapping' data. This means that a cardinal spline interpolant observes the 3 dimensional positions of a `current point' of investigation/consideration and the previous and next point. The interpolant then averages the positions using a parameter known as a *Tension* value. This *Tension* value is typically between zero and one and it acts literally like the tension in a string or wire. A higher tension value would simply yield a straight line in between the points to be splined as it would simulate an `infinitely tense' wire [19]. Interestingly enough, the cardinal spline would treat these discontinuous lines as one function much like the cubic spline, but of a higher order.

4.2. Residual Calculations

Before any comparisons or calculations could be made, it was necessary to first understand which reference points on the wing could be considered reliable or trustworthy in order to actually quantify the error. Unfortunately, Photomodeler would lack resolution in the spanwise direction (due to the limited ability of the camera angles used to capture the images, not the limitation of the program). Instead of examining all points, it was conceived that a more useful and pertinent comparison could be made by examining a few points that could define the characteristics of the wing such as torsional deformation and deflection/flapping angle. This would eliminate all issues concerning dimensionality due to the simple fact that it would not even be considered.

Before these points could be selected however, a residual calculation was performed. Photomodeler outputs its residuals in units of pixels, which to someone using Photomodeler makes sense as a reference point is defined on a single pixel, however in physical sense it is almost meaningless as a pixel count is dependent on the resolution of the camera and camera position. It was determined that in order to obtain the conversion from pixels to a physical parameter, it was necessary to re-consider Figure 9 which showed the standardized (non-translating) reference points on the physical flapping mechanism. These were separated by 6 mm center to center. Photomodeler allows for the observance of the 'pixel position' as it were for each photograph. In order to convert from pixels to mm, it was necessary to observe the pixel count in both the x and y direction between two of these reference points. The magnitude of that distance could then be applied to the pixels that separated them to gain a conversion between pixels and mm.

The results of this analysis ultimately lead into the next topic of discussion: The torsional deformation angle comparison along the span as a function of the flapper's intended angle. One conceivable issue that can be seen here is the fact that as the residuals stand, their units exist in (mm).

0.5 mm of error can be considered a small error for some applications, but it was deemed necessary to consider the actual *effect* that said errors would have on the solution in terms of 'percentage' of effect. The wing itself is 58 mm long in the spanwise direction (as seen in Figure 10), however this dimension does not represent the range of values in (mm) that the measurements for some aspects of this study would exhibit. In order to quantify the affected dimensions, it is necessary to consult Section 5.1 which describes the torsional deformation of the wing during the flapping motion by comparing the three dimensional positions of the leading and trailing edge to each other by means of a vector analysis.

Using the results of Section 5.1, a *range* of torsional deformation values could be determined (in mm) by taking the average chord of the wing (see [21]) and the magnitude of the torsional deflection (taken by subtracting the maximum and minimum values in mm). These angles could be considered a chordwise deflection (3 positions along the spanwise axis), which can be averaged to obtain a general feel for how the specimen would deflect. The maximum and minimum deflection angles could be obtained from this `average deflection along the stroke' to yield a range angle θ_{range}:

$$\theta_{range} = \theta_{max}^{avg} - \theta_{min}^{avg} \tag{1}$$

Which could then be applied to the general arc length equation:

$$s_{range} = r_{chord} * \theta_{range} \tag{2}$$

The average chord was measured to be 18.153 mm, which was gained by only considering the points associated with the torsional deformation angles. The arc length s_{range} represents the range of deflections (in mm) that will be the parameter that will be scaled against the residuals (in mm) to obtain a 'percent of effect' on the results in the following manner:

$$Residual(\%) = \frac{Residual(mm)}{s_{range}} * 100 \tag{3}$$

This percentage could then be applied to each of the positions associated with the spanwise torsional deformations. Their values will be represented as error bars in the torsional deformation data sets.

4.3. Torsional Deformation/Spanwise Deflection Angle Calculations.

It was conceived that due to the fact that a series of reference points (points in space) was the product of the data organization, it was necessary to consider the topic of vector mechanics. Theoretically speaking, a vector can be defined by two points. Should two vectors share a single point, then those vectors can ultimately define a plane. Taking the crossproduct of the two vectors that share that single point will yield a vector at the common point that is orthogonal to the plane defined by the previous two vectors. Normalization of this vector gives potential to comparison to other vectors.

If one were to do the same for a standardized, global axis system (that has been normalized), it would create a normalized, global vector for comparison. The angle with respect to the dot product of this would yield the directional cosine of the angle between them, which essentially represents the *orientation* of that plane with respect to a global axis.

The point at which the local vector was formed was the common point of the two vectors used to make the plane that existed on the flapping wing. This would be essentially indicative of the wing's deflection in the spanwise direction. The right hand picture in Figure 14 is a two dimensional illustration of this concept as it essentially uses the information presented on the left hand side of Figure 14 and applies it to a top view of the wing (a view along the spanwise direction/crossectional view).

Figure 14 serves to show the points used for this analysis and the pictorial representation of the points on the wings. Figure 15 shows the corresponding residual values for each of these points used in terms of a percent uncertainty based on total deformation.

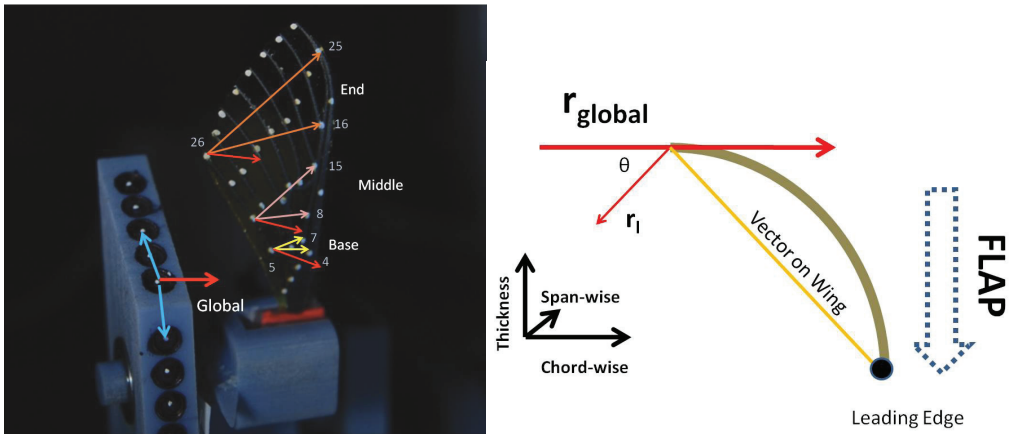

Figure 14: Torsional Deflection/Spanwise Deformation Demonstration

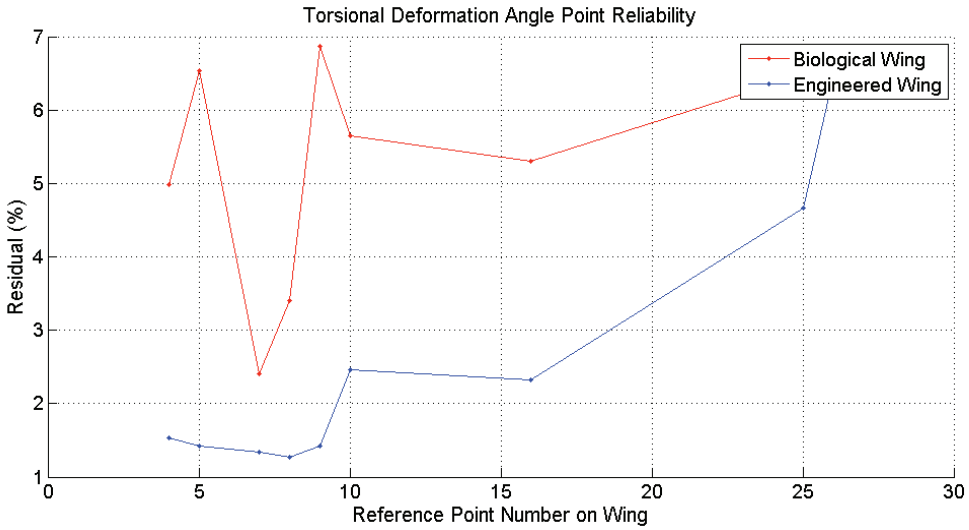

Figure 15: Torsional Deformation Angle Point Percent Uncertainty

Due to the fact that none of the points utilized for the analysis lie above 7% uncertainty, it grants confidence to the results that will be shown in Section 5.

4.4. Flapper Angular Displacement vs. Wing Angular Displacement: A Likeness to Rigid Body Motion

Similar to that of the previous analysis, it was deemed pertinent to investigate the effect of the flapping in the spanwise direction, that is to compare the angle that the flapper saw as opposed to that of what the wing emulated. This sheds light on the spanwise deflections inherent in the flapping motion and serves as a basis of comparison to what was seen in Willmont and Ellington's data (See Figure 8). This analysis is somewhat simplified in that it requires little or no effort to construct the vectors for investigative purposes. Needless to say, it is necessary to show here the vectors utilized as the normalized global vector can be represented by the y-axis alone. The vector in question would be the one represented by points 4 and 9 on the wings as it finds itself on the leading edge of the wing. This is seen in Figure 16.

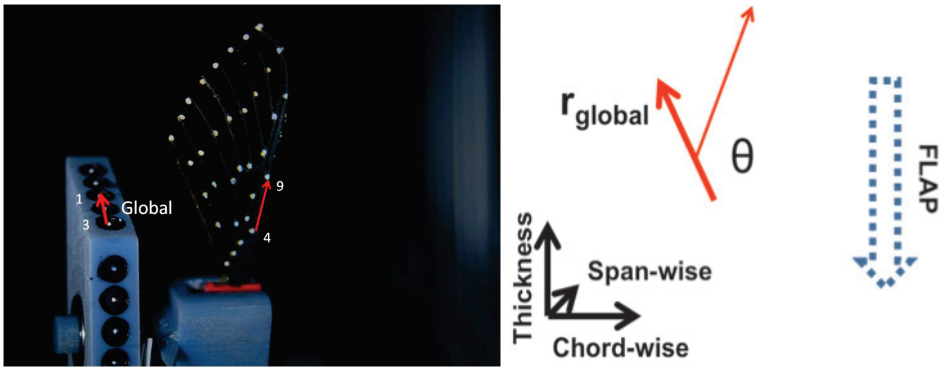

Figure 16: Angular Displacement Vector Analysis

This will be considered the final avenue of comparison between the engineered and biological wing.

5. RESULTS

The biological and engineered wings were flapped in both air and vacuum at a flapping frequency of 12.5 Hz. The same methodologies were apploed to each case allowing for data comparison. This section will reveal the results that were gained from the execution of the procedures detailed in section 3 and the mathematical manipulations in section 4.

5.1. Torsional Deformation and Angular Displacement Comparison of Biological Wing to Engieered Wing

Figure 17 depicts the comparison of both wings flapping in vacuum. Error bounds were conceived in the residual analysis from section 4.2. Upon immediate observation, it becomes clear that there is a stark difference in the behavior of the engineered wing as compared to the biological. On the downstroke, the biological wing appears to exhibit far less torsional deflection as compared to the engineered wing, which completely envelopes the bio-data. Furthermore, in the upstroke, the engineered wing appears to completely reverse direction (observe y-axis) in terms of the chordwise deflection.

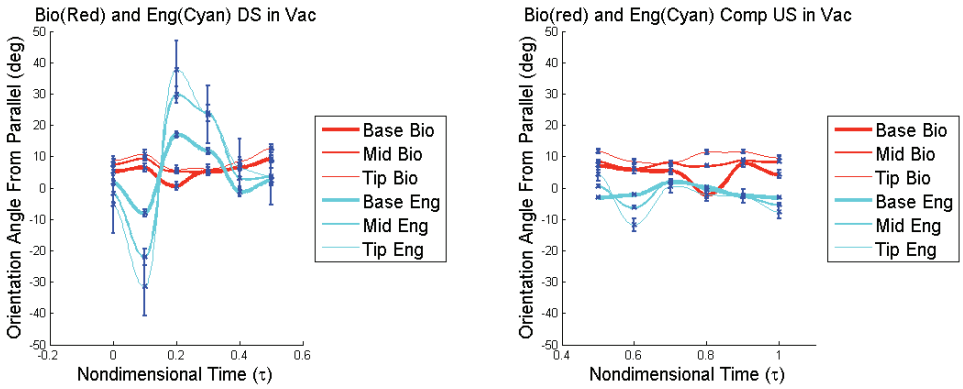

Figure 17: Downstroke (Left) and Upstroke (Right) of Biological (Red) and Engineered (Cyan) Wings Flapping in Vacuum in Terms of Local Angles of Attack Along Wingspan

It would appear that if the biological wing were taken to be the standard, the engineered wing lacks support in the chordwise direction which may be a function of construction or material properties, but in all, the performance of the engineered wing appears to overshoot what was done by the biological wing. It is helpful to compare this data with Figure 18 which depicts the same operation but in air.The presence of error in both cases makes the upstroke data difficult to discern however since all of the error bars appear to overlap. This presents challenges when attempting to draw conclusions about overall behavior of the wings when compared to each other.

Possibly one of the more important data sets that can be gleaned from this study is the comparison

between the wings in air. Figure 18 provides a glimpse of the behaviors associated with the flapping in air of both wings:

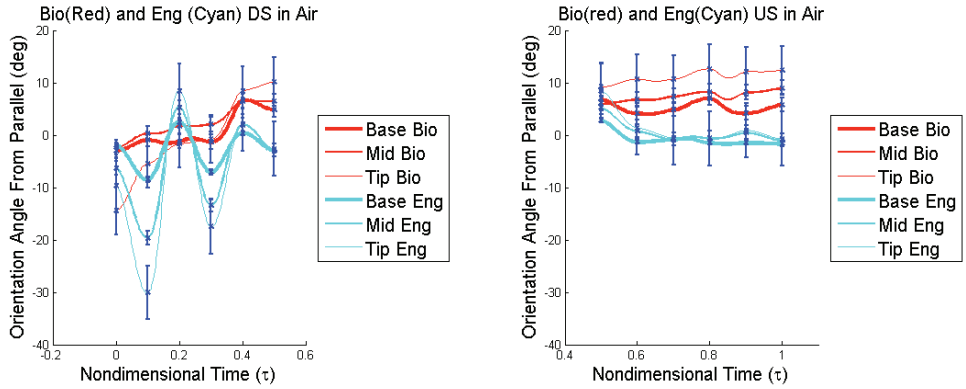

Figure 18: Downstroke (Left) and Upstroke (Right) of Biological (Red) and Engineered (Cyan) Wings Flapping in Air in Terms of Local Angles of Attack Along Wingspan

The air observation proves itself interesting simply due to the fact that the non-uniformity of the torsional deformation about the spanwise direction associated with the deflection of the wing in air is still present in both data sets as in the deflection in the spanwise direction is less uniform than in vacuum. Once again the engineered wing appears to lack the stiffness in the chordwise direction to maintain the lack of relative deflection as observed by the biological wing for the upstroke. This may be in error however due to the fact that the uncertainty associated with the upstroke proffers little reliability.

The observation of Figure 19 compares the rigid body motion of the biological and engineering wing in vacuum and in air

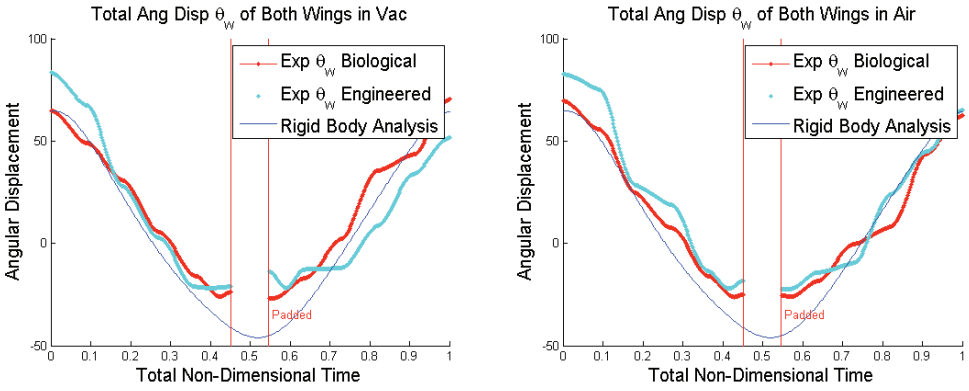

Figure 19: Vacuum (Left) and Air (Right) of Biological (Red) and Engineered (Cyan) Flapping Wings in Terms of Angular Displacement of Leading Edge

Compared to the engineering wing, the biological wing more closely emulates the rigid body motion as the engineering wing (as discussed) may have been at a disadvantage in its construction and 'not as snug' boundary condition since the biological wing appeared to have a more tight fit in the clamp and the engineered wing fit slightly easier. The 'Padded' region of the data represents the section of this study that was not captured by photogrammetry. This section would have been representative of the 'flip' between downstroke and upstroke.

5.2. Observance of Overall Wing Behavior

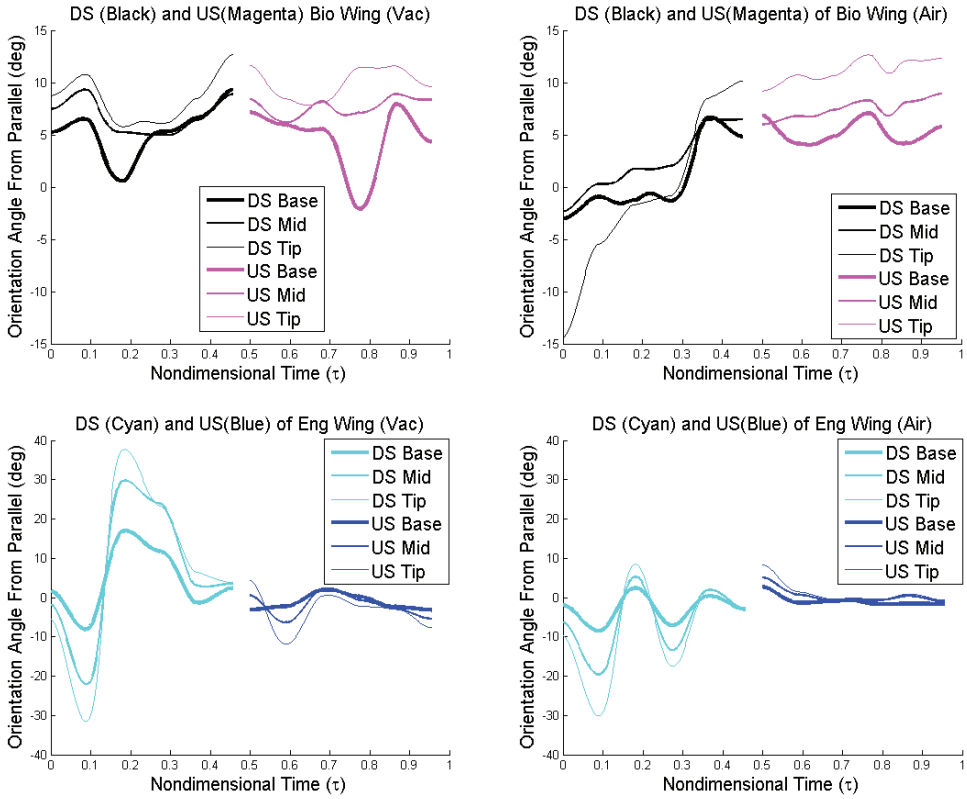

Figure 20: Overall Wing Behavior of Biological (Top Vacuum and Air) and Engineered (Bottom Vacuum and Air) in Terms of Local Angles of Attack Along Wingspan

The purpose of this section is to observe the differences in the torsional deformations of the biological wing; comparing the upstroke and downstroke. This analysis was performed for the purpose of future construction. The top portion of Figure 20 points towards the differences in stroke behavior within air and vacuum. It is important to note that the biological wing appears to have an antisymmetric motion associated with the upstroke and downstroke in air, but in vacuum this is not seen as the case as the torsional deformations seem almost symmetric. The first observation of the top of Figure 20 in the realm of vacuum, the data suggests that although not exact, the aforementioned conjecture of the asymmetric torsional deformation can be put to rest. Other than the slightly greater amplitude of deformation seen in the upstroke, it would appear that in vacuum the wing does in fact have a downstroke similar to that of the upstroke in terms of this torsional motion. The 'purely inertial' answer to the *Aeroelastic Question* would say that the wing will behave like this in air as well, wherein the symmetric downstroke/upstroke should appear not as prominently as the presence of air damping has been a continuous parameter.

In the realm of air for the biological wing, the data demonstrates problematic or challenging results. Brief inspection would indicate that the effect of air causes the biological wing to behave far differently than that of the wing in vacuum. Though flapped at the exact same frequency, air seems to illicit a unique and complex reaction from the natural wing as the downstroke exhibits a tighter, more uniform twist along the span, `scooping' the air beneath it, and the upstroke sees a non-uniform, higher amplitude twist which is indicative of allowing air to pass over the wing (as previously discussed), essentially dodging the need to move through the medium of air and exposing less surface area to the 'oncoming' velocity of air to essentially cut down on drag produced by the moving wing flapping upward.

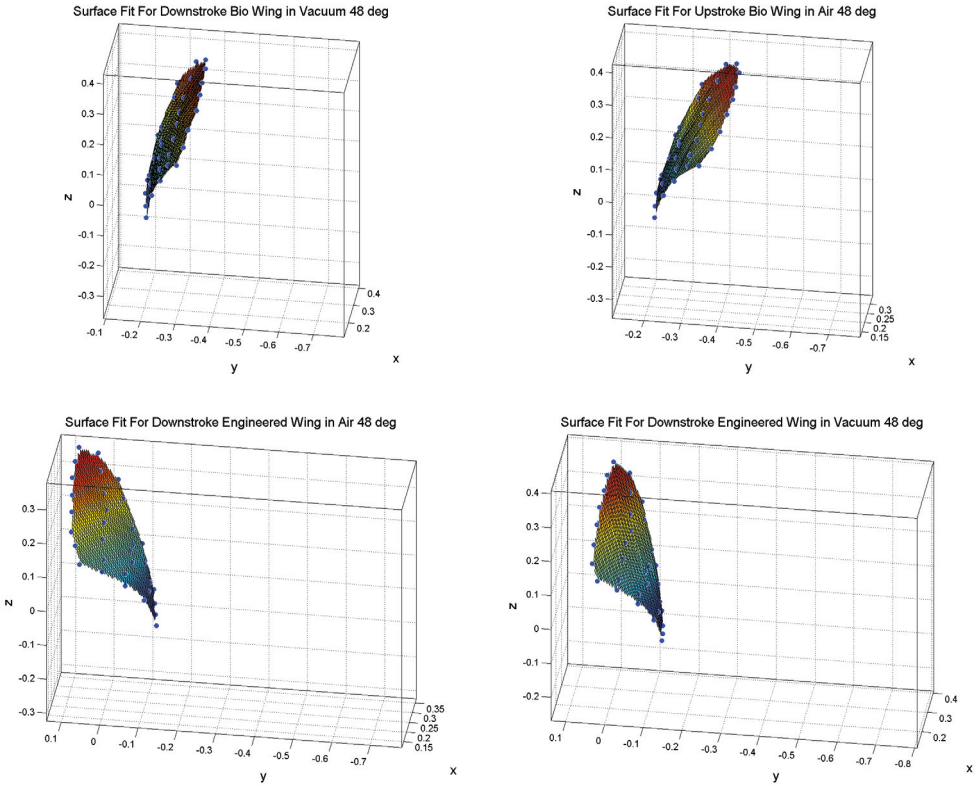

Figure 21: Overall Wing Behavior of Biological (Top Vacuum and Air) and Engineered (Bottom Vacuum and Air) Surface Fits Gained from Photomodeler (Illustrative Purposes)

This presents a rather unique problem for future engineers who wish to properly emulate the efficient, elegant motion of the wing. This is not the only study that has exposed these 'novel principles' exhibited by naturally occurring, flapping wings [21]. This comparison in air of the biological wing shown in Figure 21 brings these novel principles to light as the wing naturally exhibits this dynamic behavior- even when exposed to simplified flapping. If a higher frequency had been studied, there is no doubt that even more dramatic effects would be observed in terms of torsional deformation and deflection, paving way to future studies as materials get smarter and methods become more refined. This should grant a deeper appreciation for what was originally thought as a trivial problem as few have deemed this area of study pertinent for study and understanding.

The bottom portion of Figure 21 is shown in the similar fashion of the last two as the comparison of downstroke and upstroke of the engineered wing. It can be seen here that the deflection amplitudes here exist at much higher values than those seen in the biological wing. This is ever more evident here as the amplitudes of deflection appear to be damped by the presence of air- a behavior not observed in such magnitude by the biological wing. Here, the presence of air does not seem to affect the non-uniformity of deflection as was seen by the biological wing, but rather for the engineered wing it would appear that the uniformity is not necessarily affected nearly as much as the amplitude. The plots displayed in Figure 19 show an even clearer picture of the lack of similarity between the engineered and biological wing.

6. CONCLUSIONS

The purpose of this research study is the recognition of the complexities and structural aspects of the FWMAV. As the title of this project indicates there were two areas of interest which involve manufacturing and evaluation. This research secures the necessity for these two arenas to be coupled due to the fact that manufacturing is always subservient to the testing. Clearly this research calls for future studies to focus on more investigation into the realm of construction and mechanical considerations as was shown in the results.

The following sections will illuminate some of the specifics of the above generally stated conclusions. For this project, two wings, the separated biological wing and the biologically inspired engineered wing, were flapped at 12.5 Hz in both air and vacuum to determine their dynamic characteristics when faced with said conditions, to include a clamped, rigid base condition [1].

6.1. Manufacturing of FWMAV Wings

An efficient manufacturing technique of FWMAV wings has been developed. A single, biologically inspired MAV wing was constructed with the *Manduca Sexta* as the inspiring specimen. The main features that were chosen to be emulated were the wing/vein geometry, weight, and modal properties as these were considered very pertinent in the realm of proper emulation and construction considerations. The technique in this study utilized 3-layer, cured carbon fiber that was arranged in a 90-0-90 degree formation wherein the stiffer direction was chosen to run the span of the wing. In terms of the membranous material, 20 micron Kapton film was used due to its availability and low density. The combination of these two produced a flat, rigid wing that allowed for both spanwise and chordwise flexion yet held its rigidity and modal properties which ended up being similar to those of the Hawkmoth wing in air.

6.2. Manufacturing of Evaluation Techniques

Simplified flapping conditions were applied to a wing using an in-house constructed flapper that retained the ability to mimic both frequency and flapping amplitude. A careful kinematic analysis suggested that the flapping device came closest to emulating the angular displacement exhibited by the *Manduca Sexta* which is based on data gathered by Willmont and Ellington [16]. However, in terms of accelerations, the new AFIT flapper did not mimic the behaviors as exhibited by other, previous flappers based on a careful regression analysis executed in [22] and as can be seen on the right hand side of Figure 8. As a result of these findings, the fallibility in the realm of accelerations of the new AFIT flapper opened up a window of accessibility for study in that the amplitude of acceleration was shown to be far less than other flappers. This lack of acceleration may have in fact contributed to the ability to actually test more wings since the flapper did not overstress them.

Using Photomodeler, a program that employs algorithms based on photogrammetry and three dimensional triangulation, the three dimensional characteristics of the wing deformations were determined by effectively ‘freezing’ the flapping wing at 12 different phases within the stroke. Photogrammetry was enabled by the placement of reference points on the wings that proved non intrusive and extremely useful for data analysis. This method was applied to both a biological wing and the aforementioned engineered wing.

6.3. Modal vs. Flapping Analysis

The modal analysis proved to be very useful in providing a standardized, repeatable, and reliable process of evaluation of the two different wings that were tested. The results clearly demonstrated that though the goal of nearly matching the first resonant frequency of the biological specimen, differed from the biological wing when subjected to the flapping conditions set forth in the procedure.

6.4. The Importance of Aerodynamics

It should come as no surprise that the engineered wing requires more consideration in order to compare to the biological specimen, despite similar geometry and structural qualities (especially in the first vibrational mode). This significant finding demonstrates the wide area of inquiry that focuses on the effects of aerodynamics in this study. Trials of the biological wing in vacuum showed a passive rotation that was very similar in the upstroke as was the downstroke. This symmetry in strokes due to purely inertial loading would normally yield zero lift if that behavior was observed in air as well, but as was seen at the end of Chapter 5, this certainly was not the case.

In both cases (air and vacuum), passive rotation was observed in both wings but in air, the biological wing appeared to exhibit a non-uniform, spanwise deflection that was not observed in vacuum, effectively spreading data over a wider range of torsional deflection angles. This may be due to the presence of air in that the tip of the wing (which can be seen to be geometrically wider) presents a greater area to the medium of air, allowing the motion to have more of an effect on the deflection of the wing within that area. Furthermore, in air the wing exhibits far different torsional deflection behavior in the upstroke than in the downstroke- deforming more perhaps to allow for the ‘scooping’

of air to create lift, then leading to the reduction of negative lift in the upstroke. This behavior is significant to consider due to the fact that this naturally occurring motion was once thought to be the product of the Hawkmoth's shoulder joint/naturally occurring boundary conditions. As mentioned, this presents quite the issue for those who wish to engineer such an efficient FWMAV wherein the boundary conditions will be far less complex— owing to the abilities of the wing. For a more detailed description of the methodology and findings presented in this article, please consult [22]

ACKNOWLEDGEMENT

The authors want to thank Drs. Douglas Smith of AFOSR, Philip Beran and Richard Snyder of AFRL for their financial support over the course of this research

REFERENCES

[1] Sims, T., Palazotto, A., and Norris, A., "A Structural Dynamic Analysis of a *Manduca Sexta* Forewing," International Journal of Micro Air Vehicles, Vol. 2, No. 3, September 2010.

[2] Sims, T., A Structural Dynamic Anaysis of a Manduca Sexta Forewing, Master's thesis, Air Force Institute of Technology, Wright-Patterson AFB, OH, March 2010, AFIT/GAE/ENY/10-M22.

[3] Stanford, B., Shyy, W., and Ifju, P., *A Numerical and Experimental Investigation of Flexible Micro Air Vehicle Wing Deformations*, AIAA Paper, 2006, 4941.

[4] Michelson, R. C. and Reece, S., "Update on Flapping Wing Micro Air Vehicle Research," 13th Bristol International RPV Conference, 1998.

[5] Norris, A., Palazotto, A., and Cobb, R., *Structural Dynamic Characterization of and Insect Wing: Toward the Development of Bug Sized Flapping Wing Micro Air Vehicles*, AIAA Paper, 2010, 2790.

[6] Willmont, A. P. and Ellington, C. P., "Mechanics of Flight in the Hawkmoth Manduca Sexta I: Kinematics of Hovering Forward Flight," *Journal of Experimental Biology* 200 , 1997.

[7] Shyy, W., Lian, Y., Tang, J., Viieru, D., and Liu, H., Aerodynamics of Low Reynolds Number Flyers, Cambridge University Press, New York, NY, 2008.

[8] DeLeón, N., O'Hara, R., and Palazotto, A., "Manufacturing of Engineering Biologically Inspired Flapping Wings," *25th Annual US-Japan Composites Conference,* 2010.

[9] O'Hara, R., DeLeon, N., and Palazotto, A., "Structural Identification and Simulation of the *Manduca Sexta* Forewing," AIAA Paper, 2011, 2011 SDM Conference.

[10] Wooton, R. J., *The Insect Flight Skeleton: Towards a New Technology*? 44th AIAA Aerospace Sciences Meeting and Exhibit, 2006, AIAA 2006-36.

[11] Combes, S. and Daniel, T., "Flexural Stiffness in Insect Wings I. Scaling and the Influence of Wing Venation," *Journal of Experimental Biology*, Vol. 206, 2003.

[12] Combes, S. and Daniel, T., "Flexural Stiffness in Insect Wings II. Spatial Distribution and Dynamic Wing Bending," *Journal of Experimental Biology*, Vol. 206, 2003.

[13] Combes, S. and Daniel, T., "Into thin air: contributions of aerodynamic and inertial-elastic forces to wing bending in the hawkmoth Manduca Sexta," *Journal of Experimental Biology*, Vol. 206, 2003.

[14] Ennos, A. R., "Inertial and Aerodynamic Torques on the Wings of Diptera in Flight," *Journal of Experimental Biology*, Vol. 142, 87-95, 1989.

[15] Ennos, A. R., "Inertial Cause of Wing Rotation in Diptera," *Journal of Experimental Biology*, Vol. 140, 161-169, 1989.

[16] Willmott, A. P. and Ellington, C. P., "Measuring the angle of Attack of Beating Insect Wings: Robust Three Dimensional Reconstruction from Two-Dimensional Images," *Journal of Experimental Biology* 200, 1997.

[17] Xie, L., Wu, P., Ifju P., *Advanced Flapping Wing Structure Fabrication for Biologically-Inspired Havering Flight*, AIAA Paper, 2010, 2789

[18] Anderson, M. L., O'Hara, R. P., and Cobb, R. G., *Design, Fabrication, and Testing of an Insect-Sized MAV Wing Flapping Mechanism*, 49th AIAA Aerospace Sciences Meeting, 2011.

[19] Photomodeler, \Core Technology," 2010, URL http://www.photomodeler.com.

[20] Khan,M., "Cardinal Spline (Catmull-Rom) Spline," 2010,

URL http://www.mathworks.com/matlabcentral/_leexchange/7078-cardinal-splinecatmull-rom-spline.

[21] Weis-Fogh, T., "Quick Estimates of Flight Fitness in Hovering Animals, Including Novel Mechanisms for Lift Production," *Journal of Experimental Biology* 59 ,1973, pp. 169-230.

[22] DeLeon, N., Manufacturing and Evaluation of a Biologically Inspired Engineered MAV Wing Compared to the *Manduca Sexta* Wing under Simulated Flapping Conditions, Master's thesis, Air Force Institute of Technology, Wright-Patterson AFB, OH, March 2011, AFIT/GAE/ENY/11-M07.